Electronic Supporting Information

Heterogeneous Phosphorus-Doped WO_{3-x}/Nitrogen-Doped Carbon Nanowires with High-Rate and Long-Life for Advanced Lithium-Ion Capacitors

Juan Xu,[a] Zhenhua Liao,[a] Jiabao Zhang,[a] Biao Gao,[b] Paul K Chu[c] and Kaifu Huo [a,*]

[a] Wuhan National Laboratory for Optoelectronics and School of Optical and Electronic Information, Huazhong University of Science and Technology, Wuhan 430074, China.

[b] The State Key Laboratory of Refractories and Metallurgy, Institute of Advanced Materials and Metallurgy, Wuhan University of Science and Technology, Wuhan 430081, China.

[c] Department of Physics and Materials Science, City University of Hong Kong, Tat Chee Avenue, Kowloon, Hong Kong, China

*Corresponding Authors: E-mail: kfhuo@hust.edu.cn

Experimental section

Preparation of heterogeneous P-WO_{3-x}/NC nanowires. The heterogeneous WO_3/EDA nanowires were prepared by a modified hydrothermal method.[21] In the typical synthesis, 1 g of WO_3 was added to 75 ml of the EDA solution to form a uniform yellow solution, transferred to a 100 ml Teflon-lined stainless steel autoclave, and heated to 180 °C for 12 h. The as-obtained WO_3/EDA nanowires

were annealed at 600 °C for 2 h in Ar to form the WO_{3-x}/NC nanowires and further phosphorized at 300 °C for 2 h in the presence of $NaH_2PO_2•H_2O$ (1 g). The P-WO_{3-x}/NC product was obtained by removing the residues in the diluted acid. For comparison, WO_3 nanowires were also prepared by annealing the WO_{3-x}/NC nanowires in air at 600 °C for 2 h.

Materials characterization. Powder X-ray diffraction (XRD) was performed on the Philips X'Pert Pro super diffractometer (PANanalytical B.V., Netherlands) with Cu Kα radiation (λ = 1.54118 Å). The morphology and microstructure were characterized by field-emission scanning electron microscopy (FE-SEM, FEI Nova NanoSEM 450) equipped with an X-ray energy dispersive spectrometer (EDS) as well as transmission electron microscopy (TEM, FEI Tecnai G20). The chemical bonding and bandgap information were acquired by Raman scattering (InVo-RENISHAW), Fourier transform infrared spectroscopy (FT-IR, Bruker Vertex 80 V), ultraviolet-visible diffuse reflectance spectroscopy (UV-Vis, Lambda 35), and X-ray photoelectron spectroscopy (XPS, Kratos AXIS Ultra DLD-600 W).

Electrochemical measurement. The electrochemical properties were determined using 2025 coin-like cells. The electrolyte was a 1 M $LiPF_6$ in a 1:1 vol/vol mixture of ethylene carbonate (EC) and diethyl carbonate (DEC). In the half-cell, a Celgard 2400 film was the separator and pure Li foil served as the counter electrode. The WO_3, WO_{3-x}/NC, and P-WO_{3-x}/NC electrodes were prepared by mixing the active materials (80 wt.%), super-P (10 wt.%), and polyvinylidene fluoride (PVDF, 10 wt.%) in N-methyl-2-pyrrolidone (NMP) solution and coated on a copper foil serving as the current collector. After vacuum-drying at 110 °C overnight, the sample was pressed by a roll-press machine and punched into 6

mm diameter round electrodes with an MSK-T10 disc cutter at a mass loading of 1.7 mg cm^{-2}. The AC electrodes were prepared by mixing the active materials (90 wt.%), super-P (3 wt.%) and polytetrafluoroethylene (PTFE, 7 wt.%) and pressed on the Al foil current collector. The coin-like half-cells and LICs were assembled in an Ar-filled glove box. The P-WO_{3-x}/NC electrodes were prelithiated for three cycles at 0.1 A g^{-1} with the Li foil as the counter electrode and then assembled with the AC cathodes for the LICs tests. The anode/cathode mass ratio was 1:5.8 according to the charge balance between the anode and cathode.

The electrochemical tests were carried out at room temperature. Cyclic voltammetry (CV) and electrical impedance spectroscopy (EIS) were carried out on the CHI 660E (Shanghai, China) and Princeton applied research (Parstat4000) in the range of 10 mHz and 10^5 Hz. The galvanostatic charging/discharging (GCD) measurements and cycle-life tests performed on the half-cell and LICs were carried out on the Xinwei instrument (Shenzhen, China). The specific capacitance (C, F g^{-1}) of a LIC was calculated by Equation (1):

$$C = I/[(dV/dt)m] \approx I/[(\Delta V/\Delta t)m] \quad (1)$$

where I is constant discharge current, Δt is the discharging time, m represents the mass of the active materials, and ΔV represents the working voltage after a full discharge. The energy density (E, Wh kg^{-1}) of the LIC is calculated by Equation (2):

$$E = \int_{t_1}^{t_2} IV * dt \quad (2)$$

where I is the discharge current density (A g^{-1}), V is the working voltage (V), t_1 and t_2 are the starting/ending discharging time (s) of the LIC, respectively. The

power density (P, W kg^{-1}) of the LIC is determined from the energy density (E) and discharging time (t) according to Equation (3):

$$P = E/t \quad (3)$$

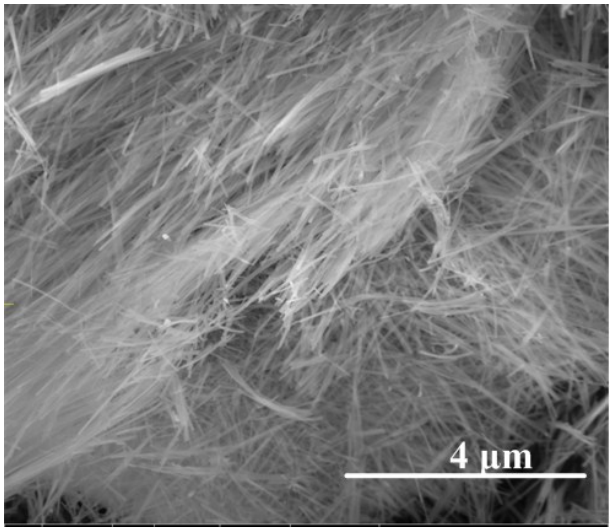

Fig. S1. SEM image of WO_3/EDA nanowires

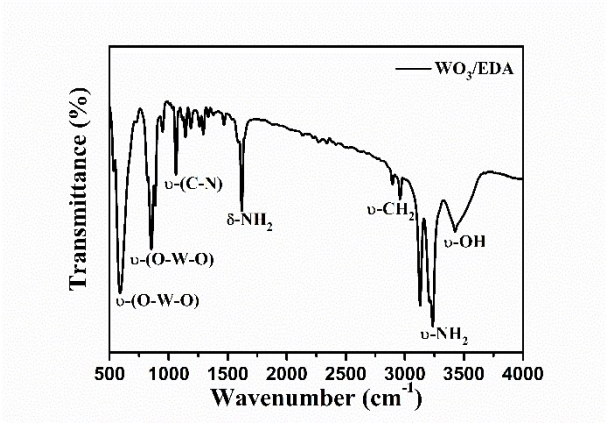

Fig. S2. FT-IR spectrum of organic-inorganic hybrid WO_3/EDA nanowires.

The presence of ethylenediamine (EDA) in the WO_3/EDA hybrid precursors was confirmed by the FT-IR spectra in Fig. S2, which displays υ-OH stretching mode (3433 cm^{-1}), υ-CH_2 bending mode (2960 cm^{-1}). The sharp peaks sat around 1620 cm^{-1} and 3245 cm^{-1}, corresponding to the δ-NH_2 and υ-NH_2 stretching modes, meaning that the interlayer organic molecules were intercalated as ammonium cations rather than neutral amines. In addition, the absorption peaks at around

590 cm^{-1} and 850 cm^{-1} could be attributed to the υ-(O-W-O) lattice vibration modes in WO_3. These results give significant evidence for the EDA molecules intercalate into the WO_3 lattice.[1]

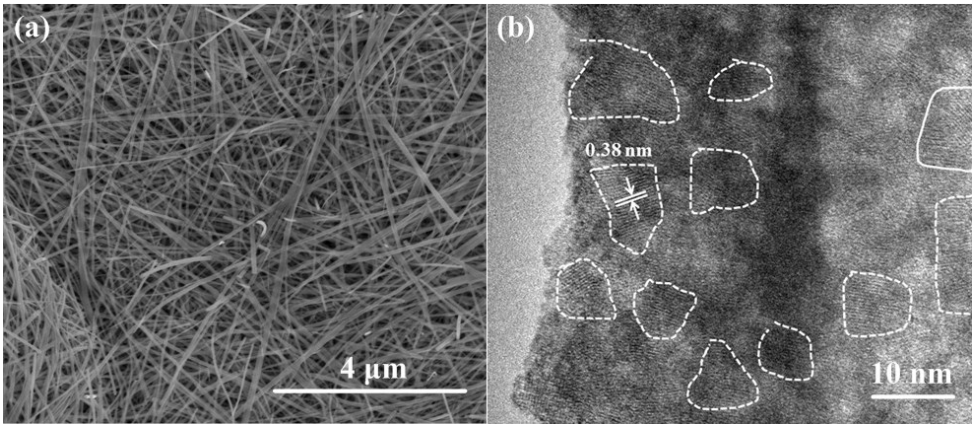

Fig. S3. (a, b) SEM and TEM image of the WO_{3-x}/NC nanowires.

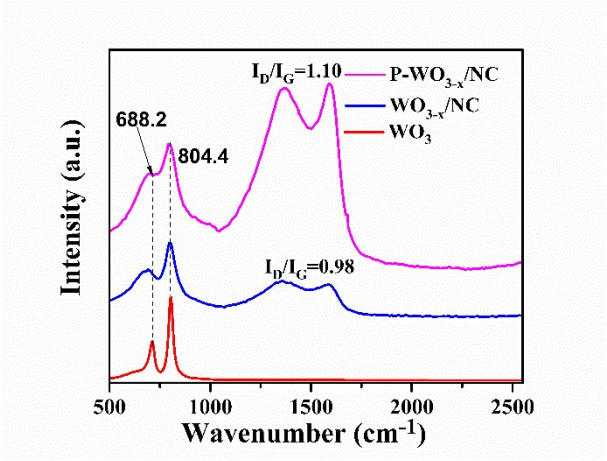

Fig. S4. Raman spectras of the P-WO_{3-x}/NC, WO_{3-x}/NC and WO_3 nanowires.

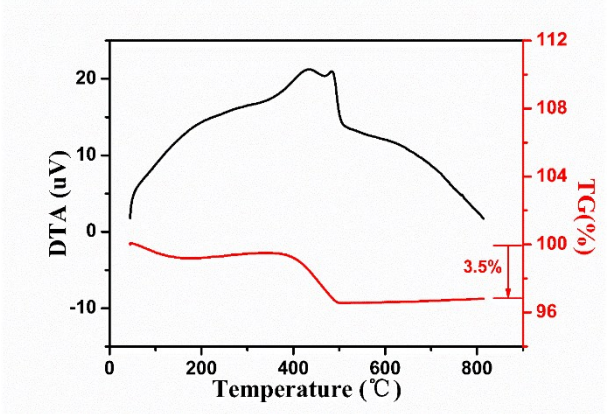

Fig. S5. TG-DTA curves of the WO_{3-x}/NC nanowires.

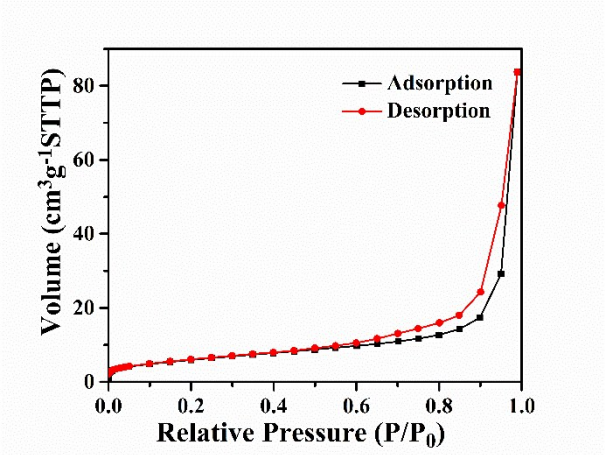

Fig. S6. Nitrogen adsorption/desorption isotherms of the P-WO_{3-x}/NC nanowires electrode.

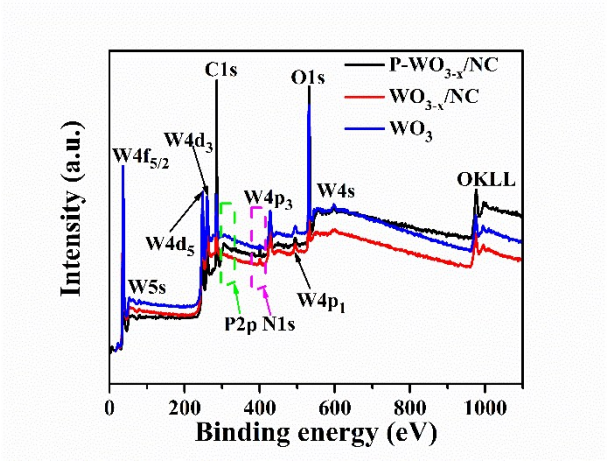

Fig. S7. XPS spectra of P-WO_{3-x}/NC nanowires; WO_{3-x}/NC nanowires and WO_3 nanowires.

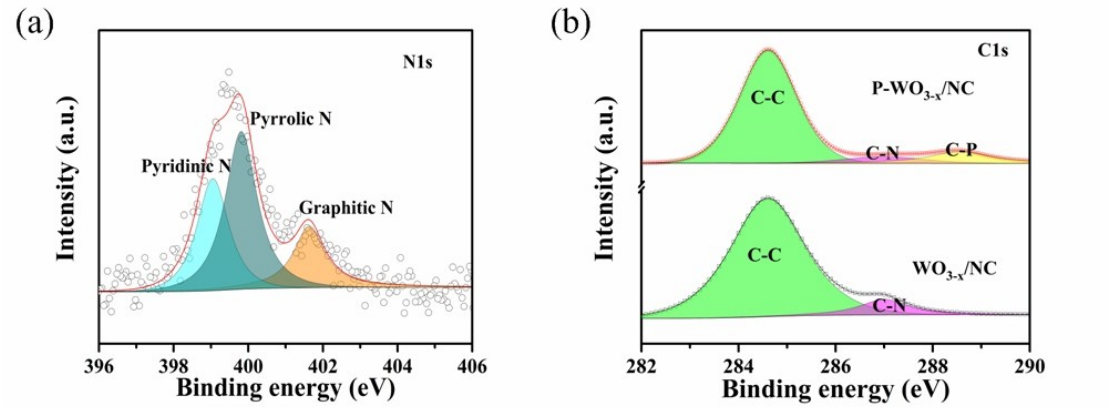

Fig. S8. (a) N 1s curves of P-WO_{3-x}/NC nanowires; C1s curves in WO_{3-x}/NC and

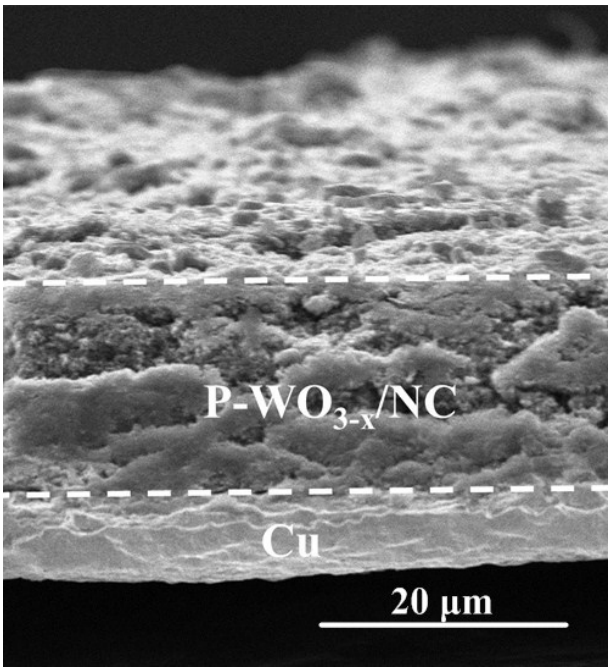

P-WO_{3-x}/NC nanowires.

Fig. S9. The thickness of the P-WO_{3-x}/NC electrodes.

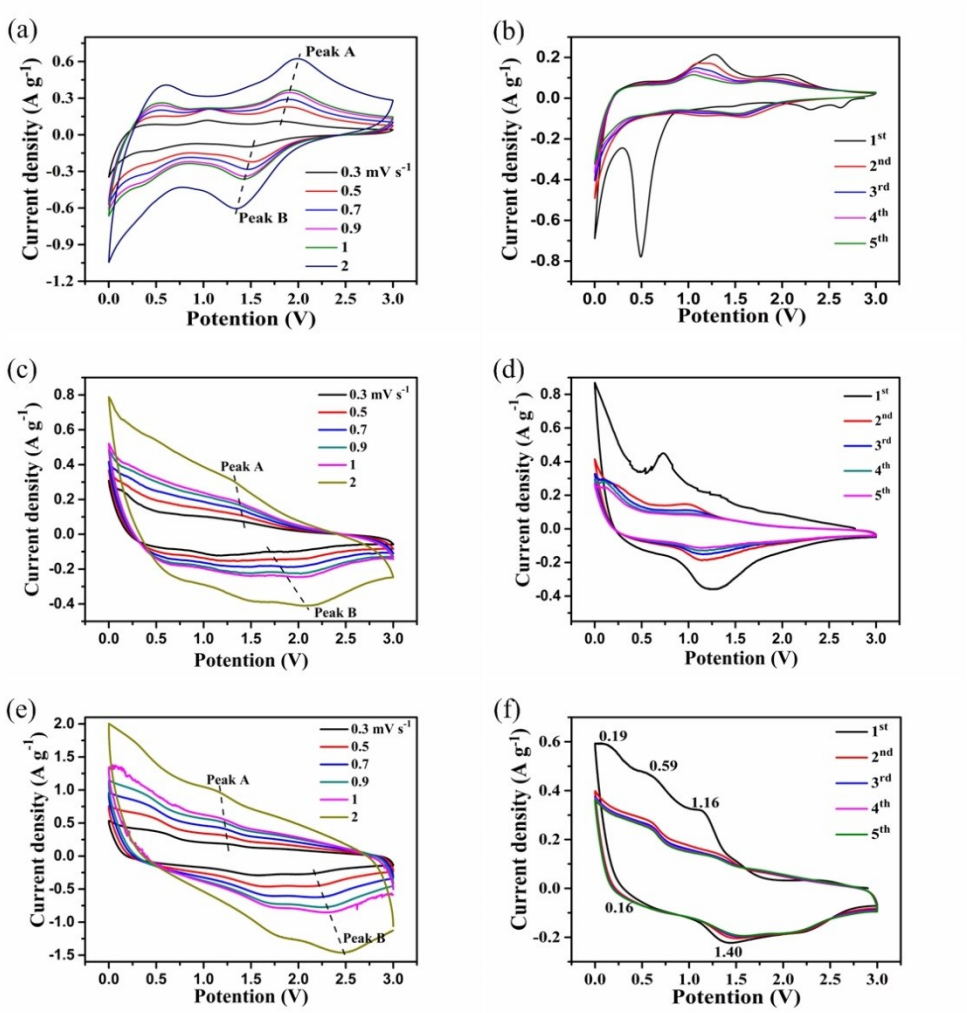

Fig. S10. (a, c, e) CV curves measured at various scan rates and at 0.2 mV s^{-1} for the first five cycles of WO_3, WO_{3-x}/NC and P-WO_{3-x}/NC nanowires electrodes, respectively.

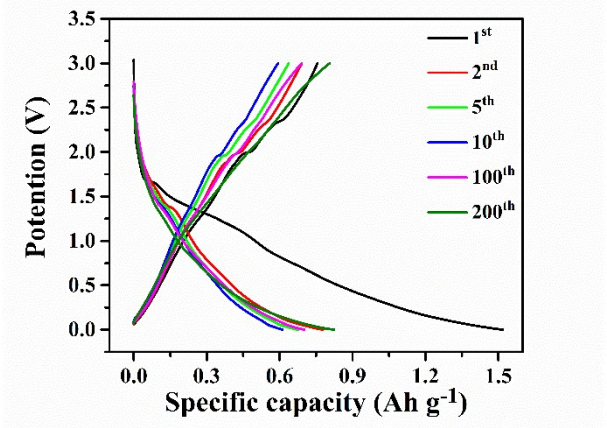

Fig. S11. The GCD curves of P-WO_{3-x}/NC nanowires electrode measured at 0.1 A g^{-1} for the 200 cycles.

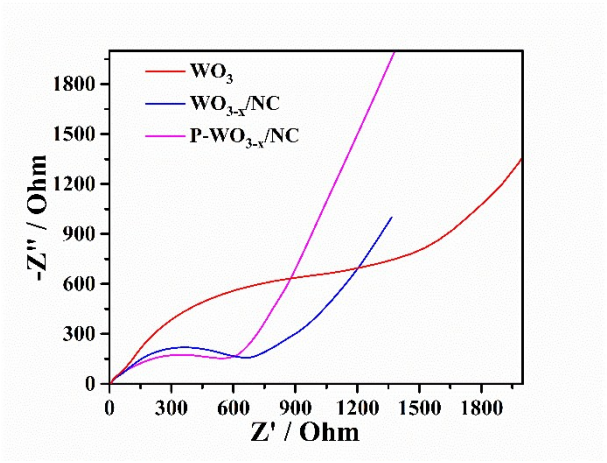

Fig. S12. The Nyquist plots of WO_3, WO_{3-x}/NC and P-WO_{3-x}/NC nanowires electrodes, respectively.

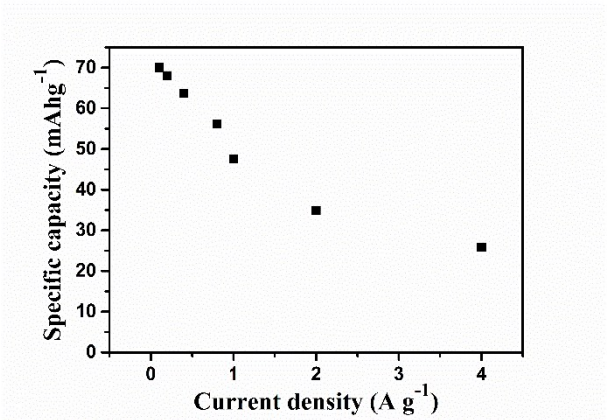

Fig. S13. Rate characteristic of AC cathode proceeds in the working window of 2-4.5 V at a series of current densities.

Table S1. Performance comparison of heterogeneous P-WO_{3-x}/NC nanowires electrode with other WO_3 composite for applications in LICs and LIBs.

Materials	Current density ($A\ g^{-1}$)	Discharge capacity ($mAh\ g^{-1}$)	Capacity after (x) cycles	Capacity at high current density ($mAh\ g^{-1}$) after (x) cycles	Ref.
WO_3 flowers	0.05	580	470 (25)	100 (0.9 $A\ g^{-1}$)(40)	[2]
WO_{3-x}/GO	0.05	1500	600 (10)	300 (1 $A\ g^{-1}$)	[3]
WO_3 hollow nanosperes	0.14	1054	320 (100)	343 (1 $A\ g^{-1}$)	[4]
WO_3 nano-ribbons	0.05	816	152 (50)		[5]
urchin WO_3/C	0.07	1229.5	508 (160)	378.4 (0.7 $A\ g^{-1}$)	[6]
WO_3 mesocrystals	0.05	1379	776 (10)	300 (0.5 $A\ g^{-1}$)	[7]
WO_3	0.14	1319	703 (10)	400 (0.7 $A\ g^{-1}$)	[8]
$W_{18}O_{49}$ nanobelts	0.1	1019.1	1284.8 (120)	527.8 (1 $A\ g^{-1}$)	[9]
WO_{3-x}/C nanosheets	0.2	1866	662 (100)	200 (1 $A\ g^{-1}$)	[10]
P-WO_{3-x}/NC nanowires	0.1	1500	806.8 (200)	490 (1 $A\ g^{-1}$)(2000)	This work

References

1 W. Li, F. Xia, J. Qu, P. Li, D. H. Chen, Z. Chen, Y. Yu, Y. Lu, R. A. Caruso and W. G. Song, *Nano Research,* 2014, **7**, 903-916.

2 Y. Qiu, G. Xu, Q. Kuang, S. Sun and S. Yang, *Nano research,* 2012, **5**, 826-832.

3 F. Liua, J. G. Kima, C. W. Leea and J. S. Im, *Applied Surface Science,* 2014, **316**, 604-609.

4 M. Sasidharan, N. Gunawardhana, M. Yoshio and K. Nakashima, *Nano Energy,* 2012, **1**, 503-508.

5 C. Lian, X. Xiao, Z. Chen, Y. Liu, E. Zhao, D. Wang and C. Chen, *Nano research,* 2016, **9**, 435-441.

6 J. Xu, Y. Y. Li, L. Wang, Q. F. Cai, Q. Li, B. Gao, X. M. Zhang, K. F. Huo and P. K. Chu, *Nanoscale,* 2016, **8**, 16761-16768.

7 X. C. Duan, S. H. Xiao, L. L. Wang, H. Huang, Y. Liu, Q. H. Li and T. H. Wang,

Nanoscale, 2015, **7**, 2230-2234.

8 P. Li, X. Li, Z. Zhao, M. Wang, T. Fox, Q. Zhang and Y. Zhou, *Electrochim. Acta,* 2016, **192**, 148-157.

9 Y. Sun, W. Wang, J. Qin, D. Zhao, B. Mao, Y. Xiao, M. Cao, *Electrochim. Acta,* 2016, **187**, 329-339.

10 K. Bao, W. Mao, G. Liu, L. Ye, H. Xie, S. Ji, D. Wang, C. Chen and Y. Li, *Nano research,* 2017, **10**, 1903-1911.